Bio-based building materials: A prediction of insulating properties for a wide range of agricultural by-products

S. Latapie, Vincent Sabathier, A. Abou-Chakra

Bio- based building materials: prediction of insulating properties for a wide range of agricultural by-products

S. Rosa Latapie*[1], V. Sabathier[1], A. Abou-Chakra[1]

[1] Université de Toulouse, INSA, UPS, LMDC (Laboratoire Matériaux et Durabilité des Constructions), 135 avenue de Rangueil, 31 077 Toulouse Cedex 04, France
*Corresponding author; e-mail: slatapie@insa-toulouse.fr

Highlights

- **Particulate thermal conductivity is calculated for a wide range of bio-aggregates**
- **Multi-scale models are consistent with aggregate morphologies**
- **Equivalent insulation performance is possible despite the diversity of the resource**

Abstract

Sustainable construction is a key solution in the light of today's climate and energy challenges. The use of plant-based aggregates in the construction sector helps to improve energy and environmental efficiency. The use of bio-based aggregates as loose-fill insulation remains limited despite the wide availability of raw materials (agricultural by-products or wild plants) and their easy implementation. One of the problems is the diversity of resources. It complicates both characterization procedures as well as the understanding and prediction of bio-material behavior. A way to overcome these obstacles is to propose a unified method which is applicable to a wide range of plant-based aggregates. This was done in this study to predict the thermal conductivity of bulk aggregates. It focuses initially on the particle scale in order to identify commonalities across a wide range of aggregates. Based on a multi-scale study it then distinguishes two different types of particulate morphologies. Particulate values of thermal conductivity - unavailable in the literature - can thus be provided over the full range of temperature and relative humidity conditions. A linear relationship between thermal conductivity and density is suggested at the particle scale while this type of relationship was previously known at the material scale. This work also demonstrate the possibility of anticipating and offering equivalent insulation performance depending on the local resource available for loose-fill insulation.

Keywords

Bio-aggregates, thermal conductivity, multiscale modelling, intrinsic variability

1. Introduction

One of the levers of the ecological transition is undoubtedly the building sector as it consumes 40% of the world's energy [1], [2] . Thus, Life Cycle Assessment (LCA) of construction materials is becoming an

ever greater concern for this sector [3] and locally available materials are to be developed and used to meet the environmental objectives [4]. Transport represents a non-negligible part of the environmental impact associated with construction projects [5], [6], [7]. In addition, manufacturing and installation techniques have to be as environmentally friendly as possible to optimize the use of bio-based resources. In this sense, using agricultural by-products as loose fill material is an efficient way of insulating buildings [8], [9], [10]. Bio-based materials also contribute to comfort in the building thanks to their passive moisture capacities [11] .

According to the FAO [12], global cereal production is approaching 3,000 million tonnes. This figure underlines the real potential of using agricultural by-products. With production set to increase further [13] , the use of agricultural by-products will become a major issue, so it makes sense to propose its use as an insulating material. Adding value to agricultural by-products is a new source of income for farmers and a springboard for the local economy [14], [15], [16]. Many cereal crops generate waste that could be used in bio-sourced building materials. However, there is a lack of data on this raw material in literature. Its variability is an obstacle to its use [17], [18] while diversity and variety of the resource constitute scientific problems [19]. To date, the thermal conductivity of plant aggregates in bulk is neither predictable nor optimizable. Time and energy consumption have to be characterized. The sample needs to be stabilized in terms of temperature and humidity. Then, to be representative, the measurement must be repeated several times, according to the recommendation of Rilem TC 236-BBM [20]. Finally, the intrinsic variability of the resource, derived from the plant world, poses a significant challenge: how can the same performance be guaranteed from one site to another when the locally available resource varies?

This article proposes a method for predicting the thermal conductivity of bulk plant aggregates at different temperatures and relative humidities. The lock represented by resource variability was removed by analyzing the similarities at the particle scale for a wide range of plant aggregates. Both based on the actual microstructure and on the macrostructure of the plant aggregate, the developed methods include several goals:

- to be applicable for all lignocellulosic aggregates
- to use easily accessible input data
- to consider the wide range of temperatures and relative humidity in use
- to provide particulate data for future modelling work.

The developed method has been validated for a dozen plant aggregates. The aim is to be able to promote and even optimize the use of agro-resources to produce bulk insulation with locally available aggregates. This is a question of proposing a "universal" prediction method for plant aggregates and is therefore an innovative step in the development of eco-materials, allowing the great variability of the resource to be overcome and yet still taken into account. This is possible because the proposed method is based on a new scale, the scale of the aggregate.

In this study, a semi-experimental protocol is proposed for obtaining an estimate of the thermal conductivity of particles of any type of lignocellulosic aggregate. It combines the results of a simple test performed on bulk particles [21] and known homogenization results. Thus, we present a general approach here, applicable and efficient for a wide variety of plant-aggregates.

Firstly, this article presents the many aggregates selected for the study and focuses on their specificities. Then models are explained and the input data are clearly defined. They are easily accessible thanks to recent work on plant aggregates [22], [23]. The model values are compared with those of the literature, for which all the input data are already known, and an extrapolation is made on certain aggregates. The relevance of this proposal is discussed. In addition, to extend use to other aggregates, a decision tree for choosing the adequate model is proposed.

Finally, the ability of our models to find the known linear relationship between thermal conductivity and density of bio-based material [24], [25], [26] is highlighted. Thanks to modelling, the same type of linear relation is demonstrated at a new scale: the particulate scale.

This study opens up new perspectives to predict and optimize insulating capacities of loose-fill insulation depending on the by-product locally available. It also provides particulate thermal conductivity values for numerous agricultural co-products which will be useful for numerous homogenization models. To date, only the thermal conductivity of hemp shiv has been experimentally measured [27] or evaluated by inverse methods [28], [29].

2. Materials

2.1 Variety of aggregates: Selection of criteria

By-products were first chosen according to their availability in the authors' region as avoiding unnecessary transportation reduces the related environmental impact. Equally important was the diversity of aggregates, to appreciate the generalizability of results. Another fundamental criterion was access to both the data required for modelling and experimental values for the same samples. This made it possible to assess the model's relevance. To evaluate its possible extension, the model was also tested on aggregates for which not all the data were known. Data were taken from the literature concerning two studies. The first one [22] gave both the necessary input data and experimental values of thermal conductivity of hemp shiv, flax shiv, sunflower pith and sunflower bark in bulk (case 1). Partial input data and thermal conductivity of aggregates in bulk were also given for six other aggregates (case 2). All measurements are considered reliable as conducted according to the RILEM TC 236-BBM procedure [20] for thermal conductivity or by the Dynamic Vapour Sorption (DVS) device for sorption isotherms [22]. The second study [30] only provided part of the input data for other samples (case 3) . Three groups of aggregates were therefore identified. For greater clarity, Table 1 summarizes the aggregates considered and the corresponding data used.

Table 1 Groups of aggregates considered depending on available data

Aggregate	Particularity
CASE 1	
Hemp shiv (HS-1)	All input data are known [21], [22]
Flax shiv (FS-1)	
Sunflower pith (SP-1)	
Sunflower bark (SB-1)	
CASE 2	
Miscanthus stem (MS-2)	
Vine shoot (VS-2)	
Coriander straw (CS-1)	

Wheat straw (WS-2) **Wheat chaff (WC-2)** **Maize husk (MH-2)**	Necessary input data are known [22] [21] except for the isotherm sorption curve. (Hypotheses are needed.)
CASE 3	
Hemp shiv (hs-3) **Sunflower pith (sp-3)**	Intra particle porosity and skeletal density of particle are known [30]. Hypotheses are needed concerning isotherm sorption curves and particulate density

This classification allowed discussion of the necessity of having access to certain input data for multiscale modelling. The following sections focus on the aggregates identified in cases 1 and 2, as experimental values are available to compare with modelled values. The aggregates of case 3 were considered only for further comparison of the modelled results (cf. section 4.1).

2.2 Chemical composition

Agricultural by-products are mainly cellulose-based since this biopolymer is the major component of plant cell walls. While the rate of crystallinity observed in cellulose is generally about 80% [31], the other main components of bio-aggregates, hemicellulose and lignin, are rather amorphous polymers [32]. In previous studies, chemical characterizations were carried out concerning the selected bio-aggregates (of cases 1 and 2) [22]. Primary components (cellulose, hemicellulose, lignin and minerals) were tested but secondary components like pectins, wax, proteins or various extractives were not. Nevertheless, cellulose was assumed to be the only chemical component with crystalline properties. Thus, it was possible to deduce the likely crystalline cellulose content for each aggregate from the cellulose content. Then proportions of crystalline and amorphous polymers in the overall solid skeleton were compared (Table 2).

Table 2. Proportions of the crystalline cellulose and amorphous biopolymers in bio-aggregates (case 1) deduced from [22].

	% cellulose	% crystalline cellulose	% amorphous biopolymers
Hemp shiv (HS-1)	55.5	44.4	55.6
Flax shiv (FS-1)	52.1	41.7	58.3
Sunflower pith (SP-1)	45.5	36.3	63.7
Sunflower bark (SB-1)	53	42.4	57.6
Miscanthus stem (MS-2)	52.8	42.2	57.8
Vine shoot (VS-2)	40	32	68

Coriander straw (CS-2)	50.4	40.3	59.7
Wheat straw (WS-2)	43.1	34.5	65.5
Wheat chaff (WC-2)	35.9	28.7	71.3
Maize husk (MH-2)	38	30.4	69.6

These values were useful to discuss the assumptions made for our model.

2.3 Macroscopic shape

Shape factors can be determined in order to evaluate and compare the macroscopic shape of the plant aggregates [33]. Circularity (C) is a dimensionless number used to appreciate the degree of roundness of aggregate. It takes values between 0 (infinitely elongated particle) to 1 (circle) and is expressed as:

$$C = 4\,\pi\,\frac{A}{P^2} \tag{1}$$

where A (mm ²) and P (mm) are the sample's area and perimeter, respectively.

The aspect ratio (R) is defined as the major to minor axis ratio and is always greater than 1. The closer the value is to 1, the more circular or spherical the particle is. The measurements of these two parameters were obtained by image analysis according to the recommendations of TC RILEM 236-BBM [34]. To assess the gap between the real macroscopic shape and a sphere for each plant aggregate, a new parameter D (deviation) was proposed as follows:

$$D = |(C - 1) + (R - 1)| \tag{2}$$

where C is the circularity and R is the aspect ratio.

For a perfect sphere, D is equal to 0. From the results of Ratsimbazafy *[22] [21]* and considering this new parameter, we can quantify the deviation of each sample from a perfect sphere (*Table 3*)

Table 3. Deviation of each plant aggregate calculated from the results of Ratsimbazafy [21], [22]

	Circularity C	**Aspect Ratio R**	**Deviation D**
Hemp shiv (HS-1)	0.34	3.30	1.64
Flax shiv (FS-1)	0.29	6.93	5.22
Sunflower pith (SP-1)	0.48	1.48	0.04
Sunflower bark (SB-1)	0.27	3.94	2.21
Miscanthus stem (MS-2)	0.28	4.63	2.91

Vine shoot (VS-2)	0.18	4.19	2.37
Coriander straw (CS-2)	0.17	6.67	4.84
Wheat straw (WS-2)	0.21	7.53	5.74
Wheat chaff (WC-2)	0.22	5.82	4.04
Maize husk (MH-2)	0.20	4.95	3.15

These results are consistent with the visual appearance of the different aggregates. Thus, the sunflower pith is objectively the most spherical granulate, while the others have rather a cylindrical or cuboid shape (Figure 1).

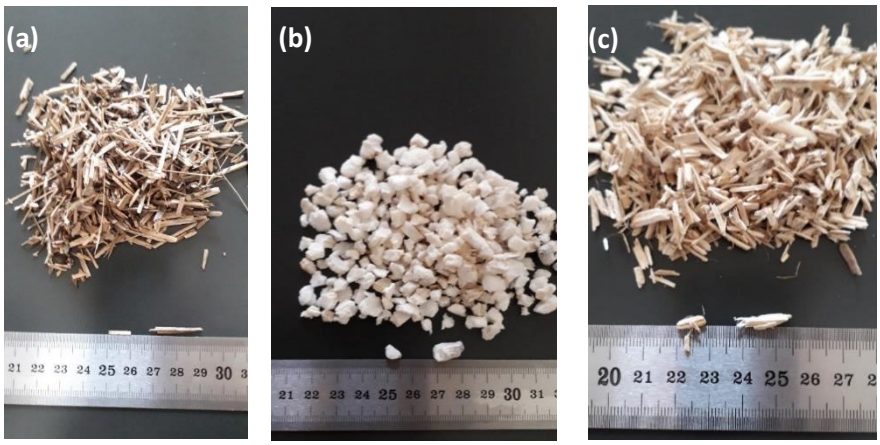

Figure 1. A selection of aggregates whose data whose data characterization was used for this study: Hemp shiv (a), sunflower pith (b), and bark (c)

The macroscopic shape of the aggregates will influence the modelling type to be considered in what follows. Two models will be studied. Their relevance to the considered aggregate will use this new "Deviation from the sphere" criterion.

2.4 Microstructure

SEM observations revealed a porous microstructure for plant aggregates, with a solid skeleton and pores of differing shapes. Skeleton densities measured by Ratsimbazafy [22] and SEM images from the literature gave us a deeper understanding of the microstructure for each aggregate. The porous structure could also be observed and characterized by X-ray tomography images [35]. Table 4 lists the references in the literature that provide an overview of the microstructural properties of the selected aggregates.

Table 4. Microstructural characteristics of plant aggregates

	Skeleton density ($kg.m^{-3}$) from [22]	**Pore shape**	**References**
Hemp shiv (HS-1)	1502	tubular	[36], [10], [37], [38],[39]
Flax shiv (FS-1)	1500	tubular	[36]
Sunflower pith (SP-1)	1536	honeycombed	[38], [40], [41]

Miscanthus stem (MS-1)	1509	tubular	[42]
Sunflower bark (SB-1)	1515	tubular	[40]
Vine shoot (VS-2)	1504	/	
Coriander straw (CS-2)	1500	/	
Wheat straw (WS-2)	1519	tubular	[36]
Wheat chaff (WC-2)	1515	tubular	[36]
Maize husk (MH-2)	1523	tubular	[35]

It should be noted that the average skeleton density for the aggregates (containing cellulose, hemicellulose, lignin, and mineral) was 1512 kg.m^{-3} while, according to a recent literature review [22], the average density of cellulose in lignocellulosic materials is 1543 kg.m^{-3}. The relative gap between these values is only 2%.

The porous structure contributes to the insulating capacity of bio-based composites [33]. Nevertheless, this porosity shows non-negligible variation [43] for the same type of aggregates and is probably impacted by factors such as the variety of the plant, the place and time of harvesting, and possible pre-treatments. Particulate porosities considered in this study were extracted from [22] and are compared to a few data available in the literature (Table 5) to highlight the spread observed in the values.

Table 5. Microstructural characteristics of plant aggregates

	Particulate porosity (%) from [22]	**Particulate porosity (%) from literature**	**Reference**
Hemp shiv (HS-1)	83.5 ± 4.8	83.0-89.3 89.3-91.3 82.5-82.17 61.5	[43] [44] [45] [30]
Flax shiv (FS-1)	71.2 ± 4.4	45.3 90.1	[30] [46]
Sunflower pith (SP-1)	96.4 ± 7.8	95.8	[30]
Sunflower bark (SB-1)	71.9 ± 4.1	53.3	[30]
Miscanthus stem (MS-2)	74.4 ± 4.3	/	
Vine shoot (VS-2)	48.2 ± 2.8	/	
Coriander straw (CS-2)	81.7 ± 4.7	/	
Wheat straw (WS-2)	71.3 ± 5.1	/	
Wheat chaff (WC-2)	71.6 ± 5.2	/	
Maize husk (MH-2)	70.9 ± 5.5	/	

Particle porosity ϕ is calculated as follows:

$$\phi = 100 . \left(1 - \frac{\rho_a}{\rho_S}\right) \quad (3)$$

where ρ_a is the particulate density of the aggregate (kg.m^{-3}) and ρ_s the density of its skeleton (kg.m^{-3}).

It must be noted that, so far, the particulate density measurement has required elaborate equipment, such as mercury intrusion porosimetry (MIP) or X-ray tomography estimation. A new method was proposed in the recent work of Ratsimbazafy [22]. It is efficient and easy to implement.

2.5 Adsorbed water

Because of their lignocellulosic nature, plant aggregates are able to absorb excess ambient water and desorb it when the humidity decreases. A hysteresis phenomenon is observable in this process [47]. Strictly speaking, the water content of the plant aggregate is different depending on whether the ambient humidity is increasing or decreasing. However, as only sorption curves are available for the aggregates in case 1 (cf. section 2.1), this phenomenon will not be considered here. Furthermore, for aggregates in case 2, an assumption had to be made since sorption curves were not available. The sorption curves plotted in the study show very similar behaviour between the different aggregates, except for sunflower pith. In the following, if no reference has been found in the literature, it is assumed that the aggregates in case 2 and 3 adsorb water in the same way as hemp shiv. Taking account of adsorbed water in multi-scale modelling requires knowledge of the volume fraction of water as a function of relative humidity, so sorption isotherm data were exploited accordingly.

3. Methods

3.1 Models developed

A triple homogenization process was used from pore scale to loose particles in order to predict thermal conductivity of plant aggregates in bulk. This multiscale study is based on the classical theory of Eshelby [48], using a Mori-Tanaka homogenization scheme [49]. Bulk aggregates are complex heterogeneous materials because the distribution of the phases is not perfectly known. The effective thermal conductivity Λ^{hom} of the equivalent homogeneous material is described as follows:

$$\mathbf{\Lambda}^{\mathrm{hom}} = \sum_{i=0}^{n} f_i . \mathbf{\Lambda}_i . \mathbf{A_i} = \mathbf{\Lambda}_0 + \sum_{i=0}^{n} f_i . (\mathbf{\Lambda}_i - \mathbf{\Lambda}_0) . \mathbf{A_i} \quad (4)$$

where $\mathbf{\Lambda}_0$ is the thermal conductivity tensor of the matrix, f_i the volume fraction of the inclusion i; $\mathbf{A_i}$ is its second order concentration tensor and $\mathbf{\Lambda}_i$ its thermal conductivity tensor.

The only values available in literature for comparison with modelled values are isotropic ones as thermal conductivity of particles in bulk is generally measured with a hot wire or hot plate (cf. section 4.2). Nevertheless, many recent studies highlight anisotropic thermal conductivity for bio-based composites [45], [50], [51]. Consequently, the anisotropy of plant particles is taken into account in one of the two models developed.

It should be pointed out that the chemical composition of the aggregates considered in this study is fairly comparable. The majority of them consist mainly of cellulose (cf. section 2.2). It was considered that their solid skeleton could be summed up as cellulose as thermal conductivity of this chemical compound is available in the literature [52]. This assumption has proved its relevance in recent work on sunflower pith [53]. In addition, analysis of the microstructure of agricultural co-products studied in the literature, whether by SEM or tomography imaging, reveals two distinct categories (cf Table 4 in section 2.4). Distinctions are made between aggregates with a honeycomb-type pore space and others with elongated and aligned pores. Macroscopically, the first ones are more spherical while the others are more elongated and can be compared to cylinders. Thanks to this analysis of both the common

points and the specific features of plant-based aggregates, two models are proposed. Model “R”, where the plant aggregate is considered to be spherical (isotropic case for each step) and model “B” where the plant particle is cylindrical (anisotropic case at the particle scale). Results from both models were compared to experimental isotropic values to assess their relevance. The overall process is summarized in Figure 2 for each model. For each homogenization step, the matrix and inclusions considered are respectively noted (m) and (i). The equivalent homogeneous medium considered in the k-th step becomes the inclusion of the heterogeneous medium considered in k+1-th homogenization.

In practical terms,the first homogenization step is carried out at the pore level to determine the effective thermal conductivity of a pore having adsorbed a certain quantity of ambient water. This pore is then included in the second homogenization step to determine the particulate dry or wet thermal conductivity. Finally, this particle becomes the inclusion in the third homogenization to gain access to the effective thermal conductivity of bulk aggregate.

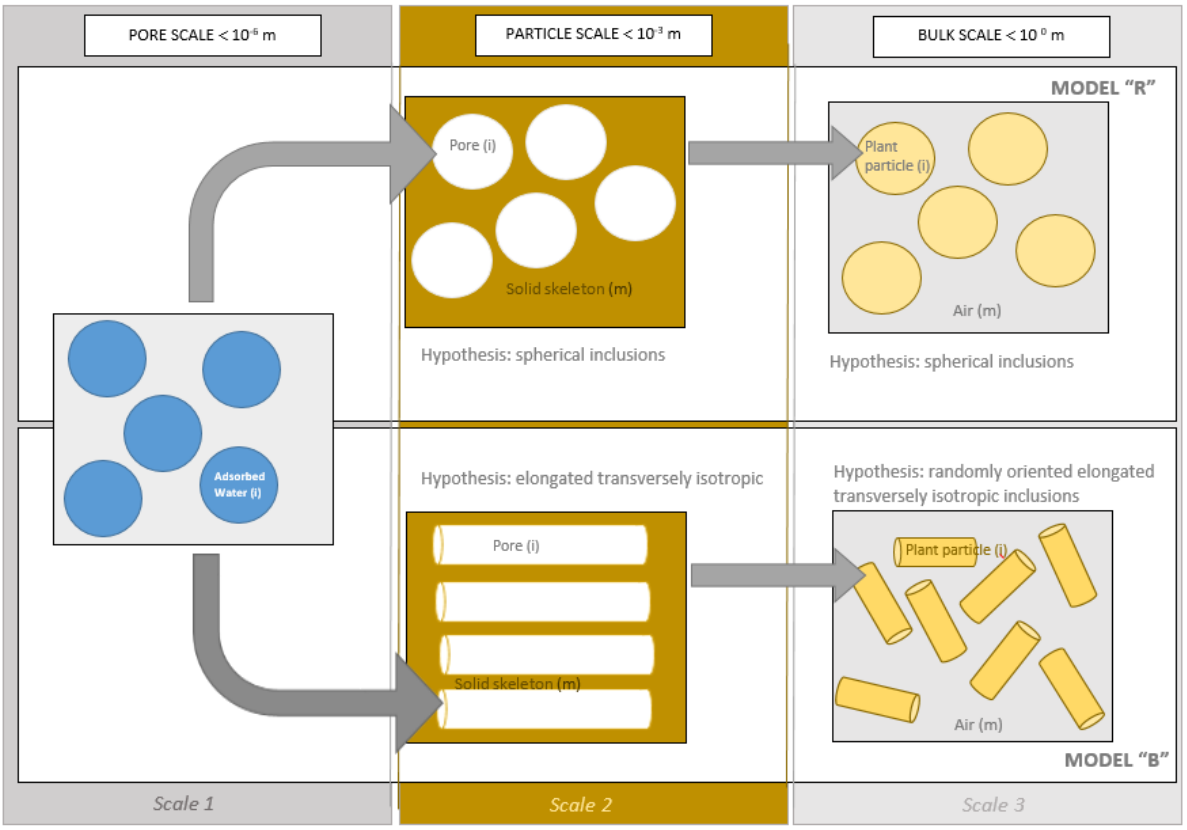

Figure 2. Description of the two models developed in this study

In model "R", thermal conductivity remains a scalar throughout the homogenization stage. In model "B", thermal conductivity is a tensor at the particle level. The formulae used for each iteration to access the effective thermal conductivity λ_{eff} are listed in Table 6. Input data from heterogeneous materials are needed for the thermal conductivity of the matrix λ_m and inclusions λ_i, and the volume fraction f_i of inclusions. The particle shape and orientation assumptions specified in Figure 2 are also considered. The iterative approach, used for the models developed here, has been validated in prior work to predict thermal conductivity of panelboards made of sunflower pith [53].

Table 6. Formulae used for each homogenization with index m for the matrix and i for the inclusion if not specified.

Iterative step	Formula	Commentary	Reference
	MODEL "R"		
Homogenization 1, 2 and 3	$\lambda_{eff} = \lambda_m + \frac{3 f_i \lambda_m(\lambda_i - \lambda_m)}{(1-f_i)\lambda_i + (2+f_i)\lambda_i}$ (5) where $\lambda_{eff} = \lambda_{pore}$ (step 1) $\lambda_{eff} = \lambda_{particle}$ (step 2) $\lambda_{eff} = \lambda_{pore}$ (step 3)	Isotropic consideration: λ_{eff} is a scalar	Rosa Latapie et al. [53]
	MODEL "B"		
Homogenization 1	$\lambda_{pore} = \lambda_{air} + \frac{3 f_{water} \lambda_{pore}(\lambda_{water} - \lambda_{air})}{(1-f_{water})\lambda_{water} + (2+f_{water})\lambda_{water}}$ (6)	Isotropic consideration: λ_{eff} is a scalar	Rosa Latapie et al.[53]
Homogenization 2	$\lambda_N = f_{pore}\lambda_{pore} + (1-f_{pore})\lambda_{skeleton}$ (7) $\lambda_T = = \left(\frac{f_{pore}}{\lambda_{pore} + \lambda_{skeleton}} + \frac{1-f_{pore}}{2\lambda_{skeleton}}\right)^{-1}$ (8) The particulate thermal conductivity is calculated with an anisotropy factor of 1.5 according Tran-Le et al. [42]. The equivalent value is based on normal and tangential values as follows: $\lambda_{particle} = \frac{\lambda_N + 2\lambda_T}{3}$ (9) where λ_N and λ_T are respectively the normal and tangential components of the thermal conductivity tensor.	Anisotropic consideration: $\mathbf{\Lambda}$ is a tensor $\Lambda = \begin{bmatrix} \lambda_N & 0 & 0 \\ 0 & \lambda_T & 0 \\ 0 & 0 & \lambda_T \end{bmatrix}$	Tran-Le et al. [29] Nguyen et al [54]
Homogenization 3	$\varphi \frac{\lambda_{air} - \lambda_{bulk}}{\lambda_{air} + 2\lambda_{bulk}} + (1-\varphi)\frac{\lambda_{particle} - \lambda_{bulk}}{\lambda_{particle} + 2\lambda_{bulk}} = 0$ (10) where φ (in %) is the porosity between particles, which is calculated from ρ_{bulk} the bulk density of particles and $\rho_{particle}$ the particulate density kg.m^{-3}) as follows : $\varphi = 1 - \frac{\rho_{bulk}}{\rho_{particle}}$ (11)		Nguyen et al.[54]

When the plant aggregates are in loose bulk, it is assumed they are not subjected to sufficient stresses to justify considering any crushing. Model B was therefore discarded for sunflower pith, since model R fulfilled the objective of taking account of the real microstructure. Consequently, the two approaches were systematically explored in order to determine the most relevant for the aggregate considered, except for sunflower pith.

3.2 Input data

Thermal conductivity of air (λ_{air}) and of water ($\lambda_{water)}$ were extracted from the work of Tsilingiris [55] and Laurent and Guerre-Chaley [56], respectively. Their variation as a function of temperature is known. The other input data used for the models are detailed for each group of aggregates (cf. section 2.1) and for each step of homogenization.

i) Homogenization 1

In this first step, the pore of the aggregate - filled with air - is the matrix and the adsorbed water is the inclusion. The sorption isotherms were therefore used to translate the mass of adsorbed water per mass of aggregate into the volume fraction of water per aggregate. The references used are listed in Table 7.

Table 7. Input data used for homogenization 1

Aggregate	f_{water}	reference	λ_{water}	reference	λ_{air}	reference
CASE 1						
Hemp shiv (HS-1)	From isotherm sorption curves of each aggregate	[22]	Digitized curves to take temperature dependence into account	[56]	Digitized curves to take temperature and humidity dependence into account	[55]
Flax shiv (FS-1)						
Sunflower pith (SP-1)						
Sunflower bark (SB-1)						
CASE 2						
Miscanthus stem (MS-2)	Hypothesis: same isotherm sorption curves as for hemp shiv (cf. section 2.5)	[22]	Digitized curves to take temperature dependence into account	[56]	Digitized curves to take temperature and humidity dependence into account	[55]
Vine shoot (VS-2)						
Coriander straw (CS-2)						
Wheat straw (WS-2)						

Wheat chaff (WC-2)			
Maize husk (MH-2)			
CASE 3			
Hemp shiv (hs-3)	Hypothesis: same isotherm sorption curves of hemp shiv as in [22] (cf. section 2.5)	Digitized curves to take temperature dependence into account [56]	Digitized curves to take temperature and humidity dependence into account [55]
Sunflower pith (sp-3)	Hypothesis: same isotherm sorption curves as for hemp shiv in [22] (cf. section 2.5)		

ii) Homogenization 2

In this step, the result of the first homogenization is exploited: the thermal conductivity of the pore is that of the inclusion. The thermal conductivity of the solid skeleton and the volume fraction of the inclusions, i.e. the pores, are also required. The volume fraction (f_i) is logically the intra-particle porosity. From this stage, it is possible to distinguish one aggregate from another although they come from the same type of plant. For the same type of plant aggregate, when the intra particle porosity is different, the particulate thermal conductivity is different. The same comments can apply to skeleton density. However, in order to avoid varying too many parameters at once, an assumption was made concerning the skeleton density of the aggregates considered in this study. The input values used in the second homogenization step are listed in Table 8.

Table 8. Input data used for homogenization 2

Aggregate	$\lambda_{skeleton}$ reference	f_i (%) reference
CASE 1		
Hemp shiv (HS-1)	Calculated from cellulose density: 1543 kg.m-3 (cf. section 2.4) [52]	83.5 ± 4.8
Flax shiv (FS-1)		71.2 ± 4.4 [22]
Sunflower pith (SP-1)		96.4 ± 7.8
Sunflower bark (SB-1)		71.9 ± 4.1
CASE 2		
Miscanthus stem (MS-2)	Calculated from cellulose density: 1543 kg.m-3 (cf. section 2.4) [52]	74.4 ± 4.3
Vine shoot (VS-2)		48.2 ± 2.8 [22]
Coriander straw (CS-2)		81.7 ± 4.7
Wheat straw (WS-2)		71.3 ± 5.1

Wheat chaff (WC-2)		71.6 ± 5.2
Maize husk (MH-2)		70.9 ± 5.5
CASE 3		
Hemp shiv (hs-3)	Calculated from cellulose density: 1543 kg.m-3 (cf. section 2.4) [52] [30]	61.5 [30]
Sunflower pith (sp-3)		95.8

iii) Homogenization 3

In this last step, the result of the second homogenization, the particulate thermal conductivity, dependent on temperature and relative humidity, is the essential input data. The volume fraction f_i of aggregates is also required. It is defined as follows:

$$f_i = \frac{V_{aggregates}}{V_{bulk}} \quad (12)$$

where $\boldsymbol{V_{bulk}}$ is the total volume of the aggregates in bulk and $\boldsymbol{V_{aggregates}}$ is that of aggregates. The volume fraction f_i is not explicitly stated in the literature. The only data currently available is bulk density. In order to be able to compare modelled values with the experimental ones for bulk thermal conductivity, the definition of density was used to modify (11) into:

$$f_g = \frac{\rho_{bulk}}{\rho_{particle}} \quad (13)$$

where $\rho_{particule}$ and ρ_{bulk} are respectively the particulate density and the density of aggregate in bulk (kg.m^{-3}). The particulate densities used in the third homogenization step are listed in Table 9.

Table 9. Input data used for homogenization 3

Aggregate	$\rho_{particle}$ (kg.m^{-3})	Reference
CASE 1		
Hemp shiv (HS-1)	248	[22]
Flax shiv (FS-1)	433	
Sunflower pith (SP-1)	56	
Sunflower bark (SB-1)	425	
CASE 2		
Miscanthus stem (MS-2)	387	[22]
Vine shoot (VS-2)	779	
Coriander straw (CS-2)	275	
Wheat straw (WS-2)	436	
Wheat chaff (WC-2)	430	

Maize husk (MH-2)	444	
CASE 3		
Hemp shiv (hs-3)	394	
Sunflower pith (sp-3)	144	[17]

It is worth noting that the density of bulk aggregates ρ_{bulk} in the third homogenization step was chosen to fit the values of the literature in order to be able to compare modelled and experimental values.

4. Results and discussion

4.1 Effective thermal conductivity of a single particle

Particulate thermal conductivity is an intermediate result in the homogenization process. However, it is interesting to give these values because, to date, only particulate thermal conductivity of hemp shiv is available in the literature [24], [27], [28], [57]. Particulate thermal conductivities are listed at 20 °C, in the dry state and 50 % relative humidity. They correspond to current conditions for measurements (dry state) and of use (under ambient conditions). Results are listed in Table 10 in order to provide an exhaustive list of values that will enable other authors to use these data, which are missing from the literature. The number of data items is large, but this also enables the differences to be appreciated between individual aggregates in the dry and wet states. In addition, it enables the effect of anisotropy on particulate thermal conductivity to be evaluated.

Table 10 Particle thermal conductivity for the plant aggregates considered in this study

Plant aggregate	**Model R**		**Model B**						**Relative gap between the models (%)**	
	λ^R particle (W.m^{-1}.K^{-1})		λ_N^R particle (W.m^{-1}.K^{-1})		λ_T^R, particle (W.m^{-1}.K^{-1})		**λ^B particle (W.m^{-1}.K^{-1})**			
	20°C Dry state	20°C 50 % RH	20°C Dry state	20°C 50 % RH	20°C Dry state	20°C 50% RH	20°C Dry state	20°C 50 % RH	20°C Dry state	20°C 50 % RH
Hemp shiv (HS-1)	0.0905	0.0908	0.1159	0.1162	0.0768	0.0771	0.0989	0.0901	0.7	0.8
Flax shiv (FS-1)	0.1439	0.1442	0.1834	0.1836	0.1211	0.1214	0.1418	0.1421	1.5	1.5
Sunflower pith (SP-1)	0.0391	0.0399	0.0452	0.0460	0.0360	0.0367	0.0391	0.0398	0	0.3
Sunflower bark (SB-1)	0.1408	0.1413	0.1795	0.1800	0.1184	0.1190	0.1388	0.1394	1.4	1.3
Miscanthus stem (MS-2)	0.1296	0.1299	0.1658	0.1660	0.1090	0.1093	0.1279	0.1282	1.3	1.3
Vine shoot (VS-2)	0.2572	0.2574	0.3094	0.3096	0.2225	0.2228	0.2515	0.2517	2.2	2.2

Coriander straw (CS-2)	0.0981	0.0984	0.1258	0.1260	0.0829	0.0832	0.0972	0.0975	0.9	0.9
Wheat straw (WS-2)	0.1435	0.1437	0.1828	0.1830	0.1207	0.1210	0.1414	0.1417	1.5	1.4
Wheat chaff (WC-2)	0.1421	0.1424	0.1812	0.1814	0.1196	0.1198	0.1401	0.1403	1.4	1.5
Maize husk (MH-2)	0.1453	0.1456	0.1850	0.1852	0.1222	0.1225	0.1432	0.1434	1.4	1.5
Hemp shiv (hs-3)	0.0941	0.0944	0.1122	0.1124	0.0832	0.0835	0.0929	0.0931	1.3	1.4
Sunflower bark (sb-3)	0.1005	0.1008	0.1173	0.1174	0.0900	0.9002	0.0991	0.0998	1.4	2.0
Sunflower pith (sp-3)	0.1042	0.1050	0.1414	0.1421	0.0852	0.0859	0.1040	0.1046	0.2	0.4
Flax shiv (fs-3)	0.1515	0.1517	0.1766	0.1767	0.1347	0.1350	0.1487	0.1489	1.8	1.8
Rape straw (rs-3)	0.1335	0.1333	0.1595	0.1596	0.1171	0.1174	0.1312	0.1314	1.7	1.4

First, the consistency of thermal particulate values is assessed by means of several findings:

- Particulate thermal values of hemp shiv are consistent with the literature [27], [28], [29], [57]
- Particulate thermal conductivity increases from dry to ambient conditions, taking account of the adsorption of water, which is much more conductive than air.
- The normal component is systematically higher than the transversal one due to the weaker connection of the solid skeleton in the transversal direction.

These values enable the insulating power of aggregates to be compared at the particle level. The general trend is that sunflower pith has a high insulating potential whatever the model. This is in line with comparative results in the literature[38], [58]. It is worth noting that the high density of the solid skeleton of the sunflower pith in the study of Chabriac et al.[30] (3400 $kg.m^{-3}$, which is almost twice that of cellulose) may explain the probably abnormally high thermal conductivity value for sunflower pith sp-3. This may be due to a particular sample or to measurement bias. Given the resource variability, it is difficult to settle this question. Straw-type aggregates have a thermal conductivity from 0.9 to 0.15 $W.m^{-1}.K^{-1}$. Vine shoot is the least promising aggregate in terms of thermal insulation. This is consistent with a relatively low porosity combined with a relatively high solid skeleton density.

The impact of variability is significant for a given aggregate type. According to modelling, with an intra-granular porosity of over 30% and a solid skeleton density of over 60%, sunflower bark SB-1 has a particulate thermal conductivity 40% higher than sunflower bark sb-3.

The anisotropy of particulate thermal conductivity explains the differences in thermal conductivity, which have been reported and studied for hemp-based composites [38], [45], [51], [59], [60]. Depending on the processing method (compaction or spraying), the preferential orientation of plant aggregates logically induces anisotropy in thermal behaviour at the material scale. From the values of the normal and tangential components given here for a wide range of aggregates, it is obvious that composites made from these aggregates will also exhibit anisotropic thermal behaviour.

In the dry state, the values of models R and B differ by an average of 1.2% at the particle scale. Under 50% relative humidity, they differ by an average of 1.3%. At this point, a conclusion could be that the

difference between the models is not significant. However, scale effects could occur at the bulk scale and the next homogenization step is different depending on the model, so neither model is favoured at this stage of the study.

4.2 Loose-fill insulation: comparison between model and experimental values

4.2.1 In dry state

The primary aim of this study was to be able to predict the thermal conductivity of plant aggregates used as loose-fill insulation from a minimum of data. The results of the triple homogenization (cf. section 3.1) were compared with those of the experimental study [21] in order to assess the relevance of the models for achieving this objective.

Maximum and minimum values for intra-particle porosity were considered to give a range of values for the modelled thermal conductivities of aggregates in bulk. Aggregates were assumed to be in a dry state [22] at the time of thermal conductivity measurement and the density was equal to the "bulk density". No compaction was assumed at the time of measurement.

i) *Model R*

Thermal conductivities calculated using the model R are presented in Figure 3 for aggregates in bulk (case 1).

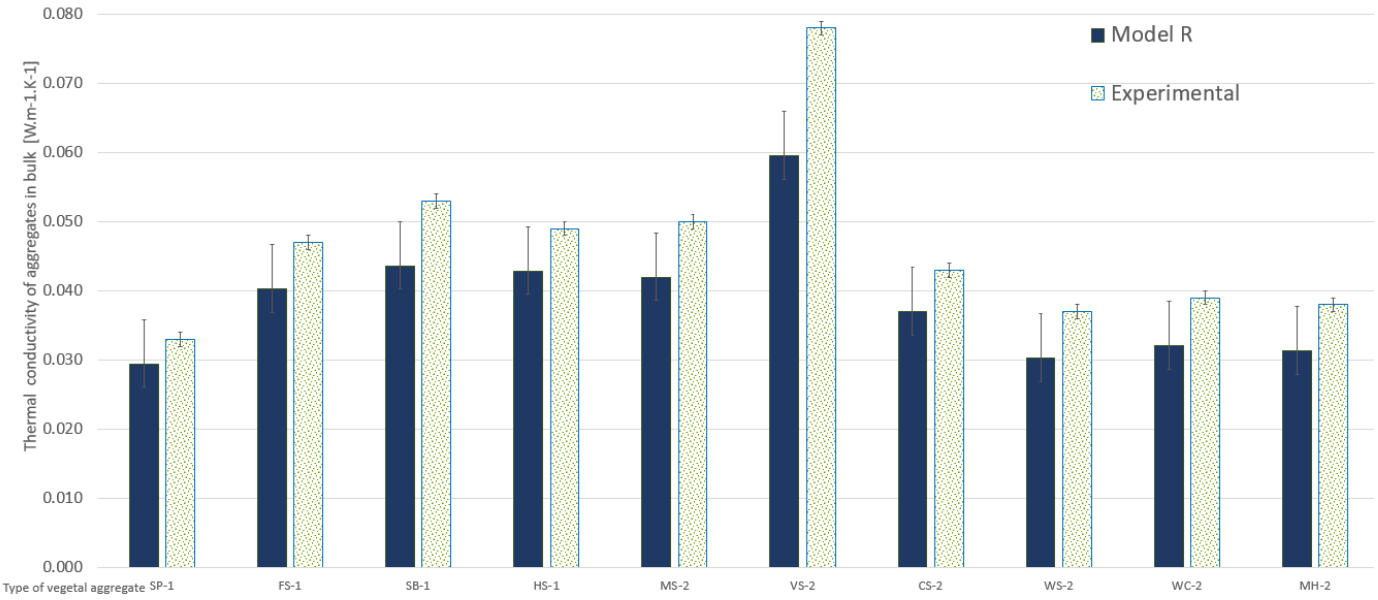

Figure 3. Experimental [21]and R-modelled values for 10 different aggregates (cases 1 and 2) at 20 °C and dry state.

The average difference between experimental and modelled values is 16%. It is worth noting that it is less than 10 % for sunflower pith. Model R, assuming spherical inclusions at each homogenization stage, therefore seems particularly well-suited to this aggregate. Nevertheless, the difference between modelling and experiment is over 20% for vine shoot. This suggests that the model is less relevant for this particular plant aggregate. This can probably be explained by a

combined effect of a microstructure very different from that assumed by the model and a rather low cellulose content compared with other aggregates.

It is also important to highlight that the model value is systematically lower than the measured value. Several explanations can be put forward to understand and correct the gap:

- Measurements were carried out on dry plant material at 20 °C, but with a relative humidity of 55 ± 5% according to the author of the study [22]. Depending on the time of measurement, the aggregates may have adsorbed water. In this condition, particle thermal conductivity and air thermal conductivity are actually higher than those considered due to this humidity.
- The plant aggregates were slightly compacted during the thermal conductivity measurement (in particular to limit the layer of air around the probe). Bulk densities could have been higher than those considered.
- For low densities, the effect of radiation can explain behaviour different from that considered here (pure conduction) [61].

Model R is easy to use thanks to the accessibility of the input data. It is particularly relevant for sunflower pith, since the spherical inclusion assumptions are in line with the real morphology of the aggregate at both microstructural and macroscopic scales. Model R demonstrates its extreme relevance and usability, first for sunflower pith but, more generally, for a wide range of lignocellulosic aggregates. This model is also relevant for a wide range of lignocellulosic aggregates, since it can predict bulk thermal conductivity with a margin of 16% in the dry state.

Finally, a comparison between the values of Model R and Model B allow the effect of the anisotropic nature of the raw material to be quantified.

ii) *Model B*

Thermal conductivities calculated with model B are presented in Figure 4 for aggregates in bulk (case 1).

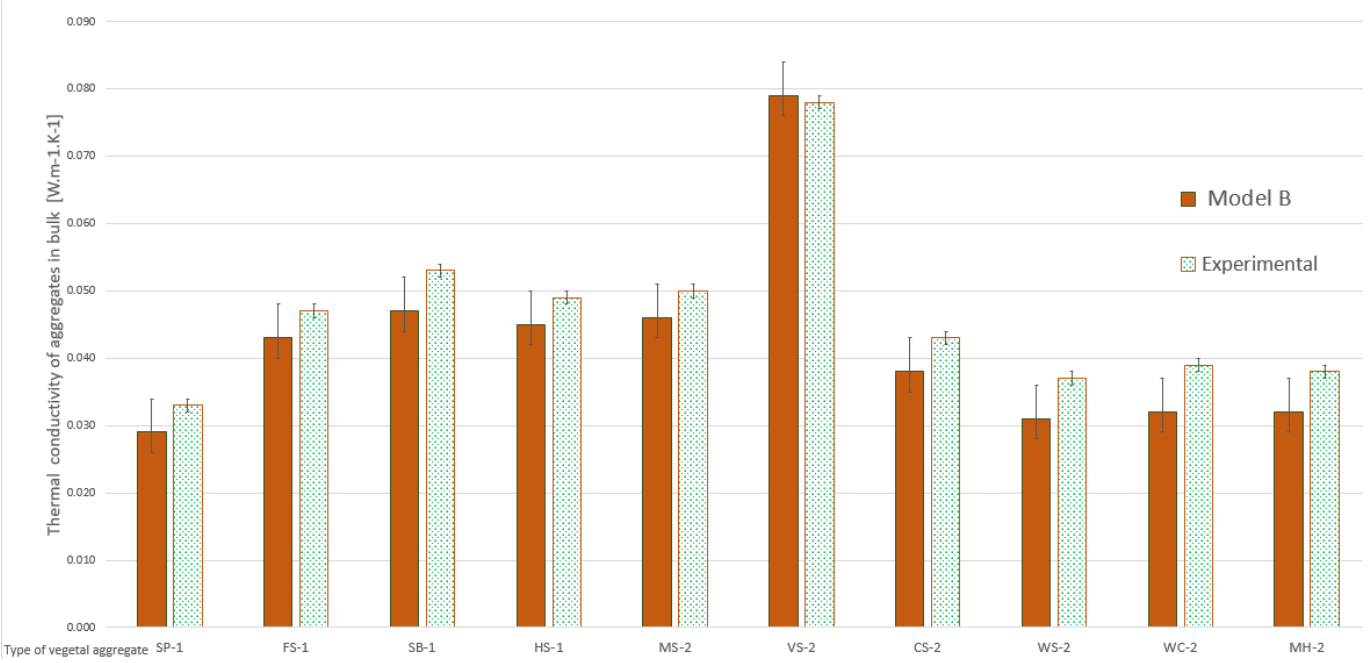

Figure 4. Experimental [21] and B-modelled values for 10 different aggregates (cases 1 and 2), at 20 °C and in dry state.

The average difference between experimental and modelled values is 11%. This model, which takes the anisotropy of thermal conductivity at the particle scale into account, is therefore relevant for all the aggregates considered here. Nevertheless, with a difference of over 12% (compared with less than 10% for model B) between the modelled value and the experimental one, it seems less relevant than model R for sunflower pith. The assumptions made here (cylindrical particle shape) deviate from the real morphology of this particular aggregate. Model B values are systematically lower than measured values (except for the shoot) as in Model R. The same explanations as above may account for this discrepancy. Model B is more complex to implement but the accessibility of the input data enable it to be used quite easily. This model is very relevant for all lignocellulosic aggregates considered in the dry state, since it can predict bulk thermal conductivity with a margin of 10%.

iii) Comparison of models

In order to further quantify and appreciate the relevance of each model, a comparison was made between the deviation, D, from the sphere of each of the aggregates (cf. section 2.2.3) and the difference between the experimental value and the value given by each model (Figure 5).

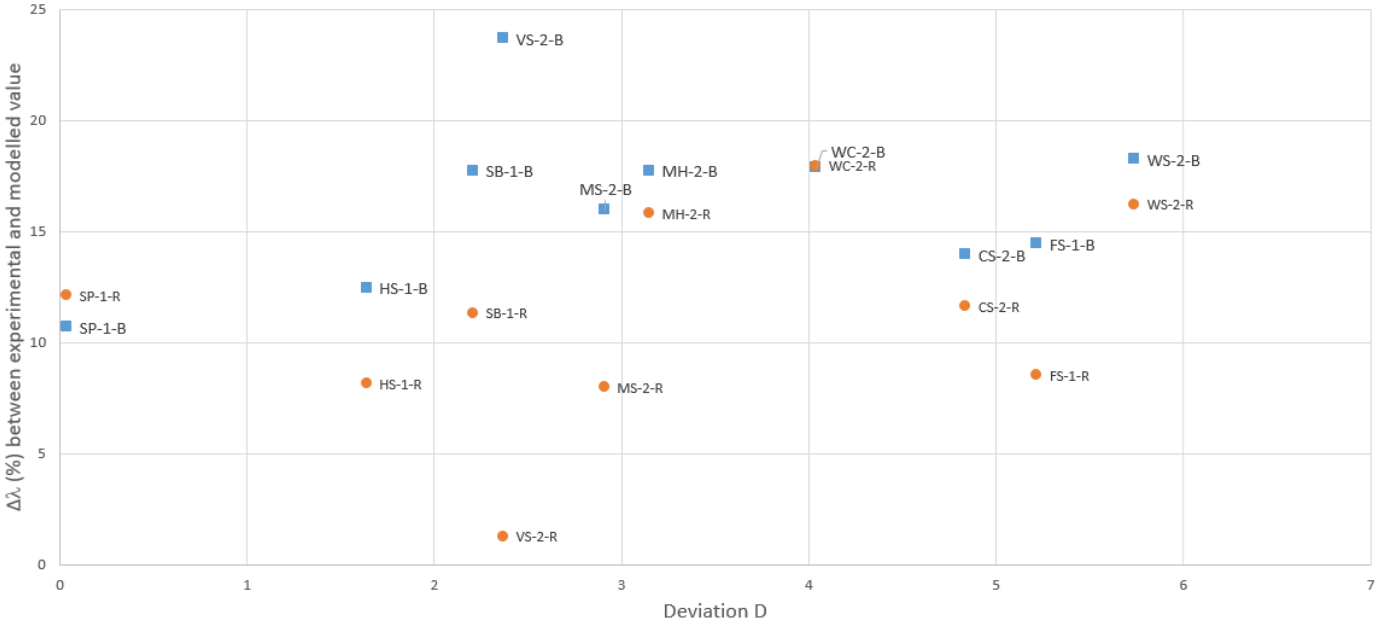

Figure 5. Experimental/model deviation as a function of Deviation D (from the sphere) for each plant aggregate and for each model (R and B).

Figure 5 shows that the difference measured between the experimental and modelled thermal conductivity values is, a priori, correlated with the deviation D defined in section 2.2.3, while model B assumes spherical inclusions at each homogenization stage. It can be concluded that the further the plant aggregate deviates geometrically from a sphere (on both microscopic and macroscopic scales), the less relevant the model becomes. Logically, model B remains more relevant for sunflower pith than model R. This is in line with its morphology. Model R is, therefore, to be recommended when considering this plant aggregate.

However, the difference between the modelled and experimental values does not systematically increase with deviation D for Model B. This model is therefore simply more relevant for cylindrical aggregates (on both microscopic and macroscopic scales). Model B is to be recommended for aggregates of this kind according to the results of this study.

4.2.2 Extended comparison

For this section, we selected bulk thermal conductivity measurements from the literature with available measurement conditions (temperature and relative humidity). These experimental values were compared with those given by our models. The input data were those used previously (cf. section 3.2) and those from the study by Chabriac et al. [30] (case 3) . Although the plant aggregates were of the same nature, they were not the same, because of the variability of the resource. Given the limited data available in the literature, only hemp shiv and sunflower pith are considered in this extended comparison of models.

i) Case of hemp shiv

Model B was applied to hemp shiv as it was considered more relevant for this aggregate (cf. Section 4.2.1). A wide range of experimental values of bulk thermal conductivities - under different temperature and relative humidity conditions - were compared with the model values obtained using the hemp-shiv HS-1 input data on the one hand and the hemp shiv hs-3 on the other (Table 11). In the case of HS-1, it is important to recall that the range of model values takes the maximum and minimum intra-particulate porosity into account (cf. Section 4.2.1). It is worth reiterating that the input data for particle porosity and particle density are different between HS-1 and hs-3 (cf. Section 3.2).

Table 11. Experimental and model values for hemp shiv in bulk under different conditions of temperature and relative humidity.

HEMP SHIV						
λ_{bulk} (W.m^{-1}.K^{-1})						
Model values		**Experimental values**				
Input data from HS -1	Input data from hs-3	Value	Ref.	Experimental conditions	Measurement method	Details
0.047-0.059	0.057	0.048	[44]	23 °C, dry state	Hot plate	Hemp shiv 0–5 mm ρ_{bulk} =135 kg.m^{-3}
0.042-0.050	0.049	0.048	[44]	23 °C, dry state	Hot plate	Hemp shiv 0–20 mm ρ_{bulk} =110 kg.m^{-3}
0.050-0.064	0.058	0.055	[10]	25 °C, dry state	Hot plate	ρ_{bulk} =153 kg.m^{-3}
0.042-0.051	0.050	0.057 ± 0.006	[63]	20 °C , dry state	Hot wire	ρ_{bulk} =114 kg.m^{-3}
0.041-0.048	0.045	0.053	[36]	23 °C, dry state	Hot wire	ρ_{bulk} =96 kg.m^{-3}
0.043-0.051	0.050	0.072 ± 0.005	[63]	20 °C , 35 % RH	Hot wire	ρ_{bulk} =114 kg.m^{-3}
0.047-0.053	0.057	0.0545	[64]	25 °C, ambient RH (assumption: 60% RH)	Hot plate	ρ_{bulk} = 134.8 kg.m^{-3}
0.046-0.057	0.069	0.0542	[64]	25 °C, ambient RH (assumption: 60% RH)	Hot plate	ρ_{bulk} = 164.5 kg.m^{-3}

These data show a high degree of variability. The thermal conductivity of bulk hemp shiv varies experimentally from 0.048 to 0.072 W.m^{-1}.K^{-1} for a bulk density from 96 to 153 kg.m^{-3}. This represents

a 50% variation in insulating capacity. The model predictions are in line with this variability, as thermal conductivity is evaluated as increasing from 0.041 to 0.064 $W.m^{-1}.K^{-1}$, i.e. a variation of 56%, when input data from HS-1 is used. Using input data from hs-3 gives a variability of only 30% in bulk thermal conductivity. This is explained by the fact that the intrinsic variability of the aggregate is not considered in this case; only the average intra-particulate porosity is considered. These results show the importance of evaluating and considering the range of particulate porosity rather than the average value, which masks the great variability of the raw material.

In addition, it is interesting to compare the average dry state thermal conductivity values given by the model with the average of the experimental values (Figure 6).

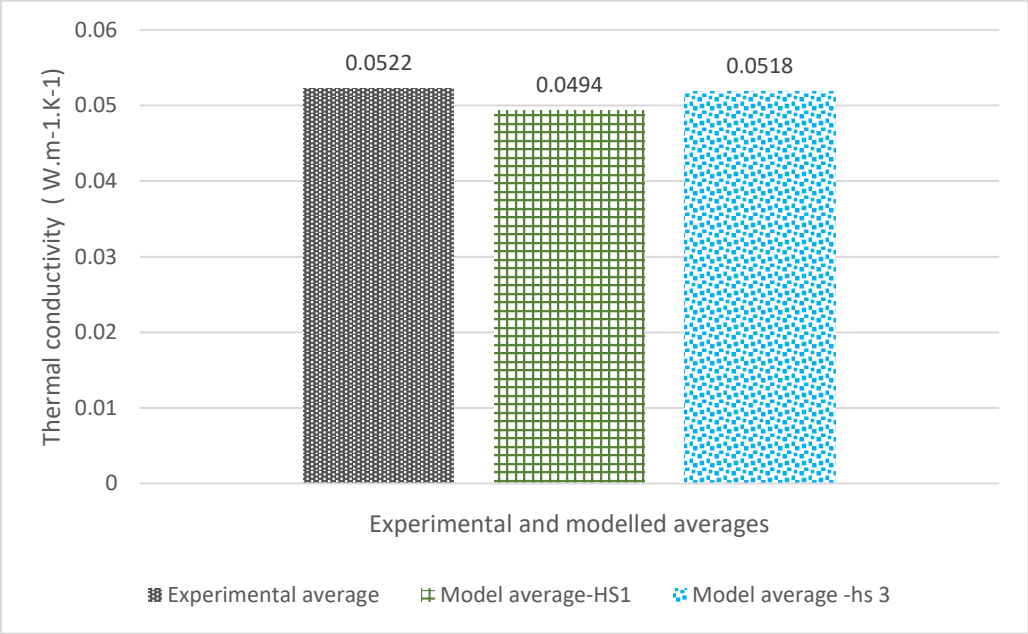

Figure 6. Experimental and modelled averages of thermal conductivity for hemp shiv in bulk in the dry state

When the average of predicted values over the range of bulk densities from 96 to 153 $kg.m^{-3}$ is considered, the model demonstrates its extreme relevance for the dry state. The maximum deviation between the average of modelled values and the average of experimental ones is 5%.

On the other hand, it is more difficult to draw conclusions concerning thermal conductivity prediction under certain relative humidity conditions, given the limited experimental data. Nevertheless, the model values differ from the experimental values by 25% with HS-1 input data and by 12% with hs-3 input data on average. This highlights the significant impact of particle density on the output data. It is therefore fundamental input data.

Our results were compared with those of several studies in the literature and highlighted the need to know the ranges of both the particulate density and the intra-particulate porosity for the aggregates considered when using model B.

Finally, to reflect the material's behavior in a wet atmosphere, the adsorbed water is considered from the pore scale in agreement with the sorption isotherm of the aggregate. This inevitably impacts the results of successive homogenizations. According to our models, bulk thermal conductivity increases on average by 8% between the dry and wet states (60% RH) for hemp shiv in bulk. These averaged figures should be taken with caution: to be as rigorous as possible, it would be necessary to have the measurement on the same sample in dry and wet state humidity because of the variability of the resource.

ii) Case of sunflower pith

Model R was applied to sunflower pith as it was considered more relevant for this aggregate (cf. section 4.2.1). A range of experimental values for bulk thermal conductivities - under different temperature and relative humidity conditions - were compared with the model values found with the sunflower pith SP-1 input data on the one hand and the sunflower pith sp-3 on the other (Table 12).

SUNFLOWER PITH						
λ_{bulk} **(W.m^{-1}.K^{-1})**						
Model values		**Experimental values**				
Input data from SP -1	Input data from SP-3	Value	Ref.	Experimental conditions	Measurement method	Details
0.028-0.046	0.034	0.051	[64]	23 °C, ambient RH (hypothesis: 60% RH)	Hot plate	ρ_{bulk} = 20 kg.m^{-3} ($\rho_{aggregate}$ = 35 kg.m^{-3})
0.027-0.041	0.033	0.036 ± 0.001	[65]	23 °C, dry state	Hot wire	ρ_{bulk} = 15.9 kg.m^{-3}
0.027-0.039	0.032	0.050	[58]	25°C, 60% RH	Hot wire	ρ_{bulk} = 14 kg.m^{-3}

Table 12. Experimental and model values for sunflower pith in bulk under different conditions of temperature and relative humidity.

As in the case of hemp shiv, these data show a high degree of variability. The thermal conductivity of bulk sunflower pith varies experimentally from 0.036 to 0.051 W.m^{-1}.K^{-1} for a bulk density from 14 to 20 kg.m^{-3}. This represents a variation in insulating capacity of about 40%. The model predictions overestimate this variability, as thermal conductivity is evaluated from 0.027 to 0.046 W.m^{-1}.K^{-1}, i.e. a variation of more than 60 % from when input data from SP-1 is used. Using input data from sp-1 gives a variability of less than 10 % in bulk thermal conductivity. The high porosity of this aggregate (over 95% in the case of SP-1 and sp-3) implies that variations in bulk density have less impact on bulk thermal conductivity than in the case of hemp shiv (the particle porosity of which is closer to 80%). The proportion of air in this extremely porous material is so high that the impact of conduction in the solid skeleton is very low.

Model values in Table 12 are systematically lower than experimental ones when modelling with sp-3 input data. The difference is almost 25%. With SP-1 input data, the difference is about 22%. Nevertheless, it should be noted that the model values are within the range of the experimental value in one of the cases reported [65]. If the particulate density is corrected by applying that of the sunflower pith studied by Magniont [64] as input data, the model's predictions are improved. As an

illustration, using a particle density of 35 kg.m^{-3} and assuming an intra-particle porosity of 90 $\pm$ 5 %, the prediction of thermal conductivity is 0.036-0.051 W.m^{-1}.K^{-1} under 60% RH and 23°C, and 0.036-0.052 W.m^{-1}.K^{-1} under 60% RH and at 25 °C. This is consistent with the experimental values of 0.051 and 0.050 W.m^{-1}.K^{-1} [58], [64]. To make good predictions, the model needs reliable input data on the sunflower pith used for measuring.

From this extensive comparison of our modelled values with experimental values, it can be concluded that the fundamental input data required to ensure the model's relevance are:

- the range of intra particulate porosity.
- the particulate density.

4.4 Thermal conductivity versus density

4.3.1 At the bulk scale

The literature reports a linear relationship between measured thermal conductivity $\lambda_{bulk\ exp}$ and bulk aggregate density ρ_{bulk} [21] as follows:

$$\lambda_{bulk\,\exp 1} = 0.0001\ \rho_{bulk} + 0.0311 \qquad (14)$$

Under the same conditions (dry state, 23 °C), Viel [36] found a similar relation according to experimental values from a wide range of bio-aggregates:

$$\lambda_{bulk\,\exp 2} = 0.0001\ \rho_{bulk} + 0\ .0398 \qquad (15)$$

These correlations are based on experimental results. In order to assess the predictive potential of our models, the thermal conductivity of ten dry bulk aggregates (cases 1 and 2) at 23°C was plotted as a function of bulk density. Acknowledging the findings of the previous sections, Model B was used for sunflower pith and Model R for the other plant aggregates to ensure a coherent approach. The results are presented in Figure 7.

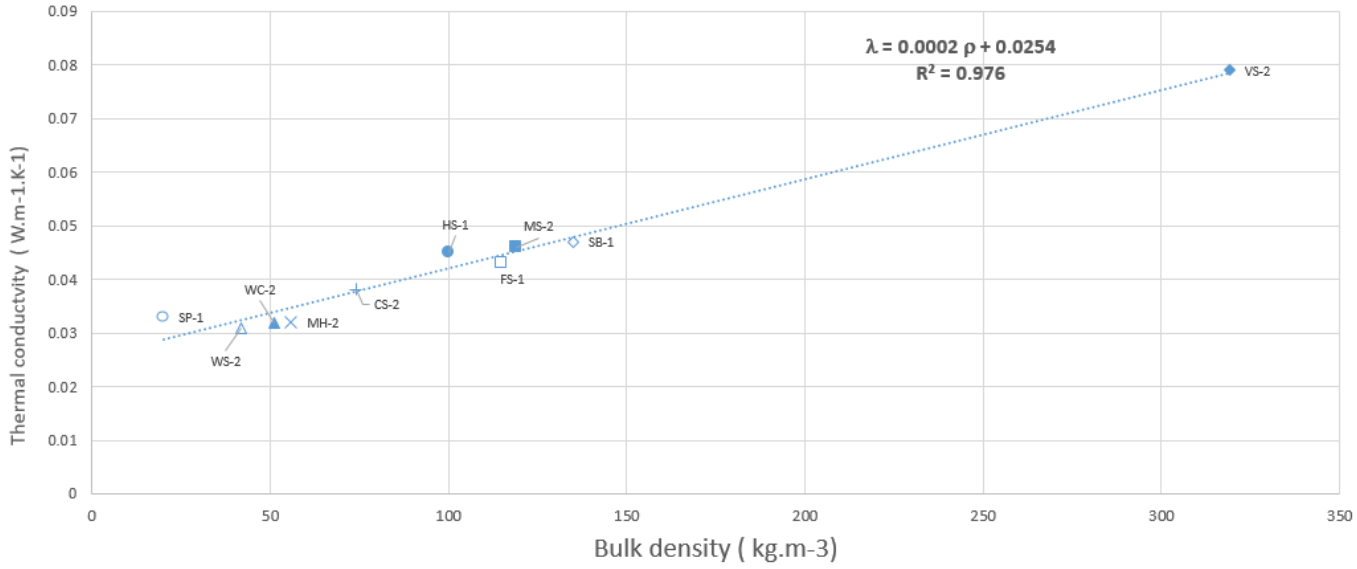

Figure 7. Plant aggregates' thermal conductivity as a function of their bulk density: modelling values at dry state, 23 °C.

The linear relationship obtained with modelling is in good agreement with that reported in the literature:

$$\lambda_{bulk\ model} = 0.0002\ \rho_{bulk} + 0.0254 \quad (16)$$

where $\lambda_{bulk\ model}$ (W.m^{-1}.K^{-1}) is the thermal conductivity of bulk aggregates and ρ_{bulk} (kg.m^{-3}) the bulk density.

According to the model equations, the y-intercept represents the case where the plant aggregate volume fraction is zero. This is the borderline case where there is only air. From this perspective, the value we obtained by modelling is entirely consistent, since the thermal conductivity of dry air at 23°C is 0.026 W.m^{-1}.K^{-1} [55] . The values of 0.0311 and 0.0398 W.m^{-1}.K^{-1} - obtained from experimental data – differ by 20% and 50 %, respectively, from this value.

Our model is therefore efficient for predicting the thermal conductivity of bulk insulation from bulk density for a wide range of cellulosic aggregates. It can thus anticipate and optimize the thermal conductivity of several aggregates from a loose or compacted implementation.

To progress further, a comparison is made with the relations commonly given for bio-based concretes (bio-aggregates and binder) [24]:

$$\lambda_{bio-based\ composite} = 0.0002\ \rho_{composite} + 0\ .0194 \quad (17)$$

where $\lambda_{bio-based\ composite}$ (W.m^{-1}.K^{-1}) is the thermal conductivity of bio-based composites (vegetal concretes) and $\rho_{composite}$ (kg.m^{-3}) their density.

The same remark applies to the intercept as previously. In this case, it differs by 30% from the thermal conductivity of air. In addition, discussion is needed on a possible impact of the binder. Comparing relations (16) and (17) may demonstrate that a difference of binder only leads to a translation of the line (same slope).

Finally, it should be pointed out that experimental linear relationships cannot be exploited to predict thermal conductivity over the wide range of conditions of use (temperatures and relative humidity). Given the resource variability and the time necessary for characterizations, modelling is a fundamental and necessary tool for predicting thermal conductivity of bio-based building materials.

4.3.2 At the particle scale

The linear relationship between thermal conductivity and density has been highlighted in the literature for both aggregates in bulk [21] and bio-based composites [66], [67]. In the process of this multi-scale study, identification of a possible linear relationship at the particle scale was attempted as models give access to particulate thermal conductivities (cf. section 4.1). The particulate thermal conductivities as a function of the particulate densities have been plotted in Figure 8.

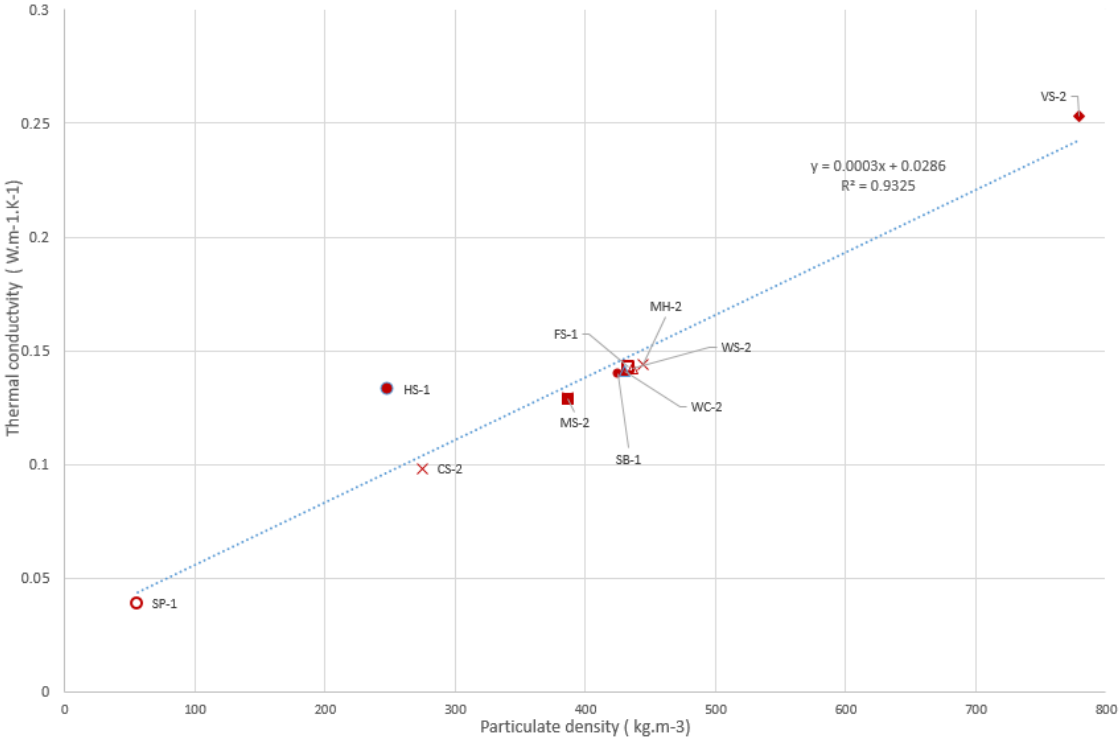

Figure 8. Particulate thermal conductivity as a function of particulate density: modelling values in dry state, 23 °C.

The results demonstrate that the linear relationship between thermal conductivity and density can be written from the particle scale. As in the previous section, the y-intercept corresponds to the value of the thermal conductivity of dry air at 23 °C:

$$\lambda_{particle} = 0.0003\,\rho_{particle} + 0.0286 \quad (18)$$

where $\lambda_{particle}$ (W.m^{-1}.K^{-1}) is the particulate thermal conductivity and $\rho_{particule}$ (kg.m^{-3}) its density.

The denser the particle is, the higher is its thermal conductivity. This is logical given the mode of propagation of heat by conduction. It is clear that this link is linear at the particle scale. Consequently, any variation in the particulate density has a strong impact on the particulate thermal conductivity and therefore on the insulating capacity of the material made of this plant aggregate.

Thanks to these results, it now possible to quantify the effect of any treatment (chemical or retting) or ageing of the particulate solid skeleton [68] (change in particulate density) on the thermal conductivity of plant aggregates through the effect on particle density. It would also be interesting to study the impact of the plant variety, harvesting period or retting on the physicochemical composition of the agricultural co-product that impacts particulate density. Thus, both prediction and optimization of its insulating capacity could be considered.

4.5 Equivalent walls

It is interesting to compare insulating properties on a particulate scale (cf. section 4.1) or on a bulk scale [69]. However, in order to offer equivalent insulation depending on the local availability of raw material, it is helpful to consider thermal resistance. Thanks to the models developed in this study, it is possible to propose thermally equivalent walls depending on the local availability of aggregates. The thermal resistance of 7 m^2.K / W was chosen as it corresponds to the value recommended for lost attic space in France, where new thermal regulations have just come into force (RE 2020) [70]. Considering

this target value for thermal resistance, the thickness of bulk aggregate required was determined (at 23 °C and in the dry state). The results are summarized in Table 13.

Plant aggregate	Bulk density considered [kg.m^{-3}]	Thickness required for loose-fill insulation to obtain 7 m^2.K / W according to modelling [cm]
HS-1	100	31.5
FS-1	115	30.1
SP-1	20	20.3
SB-1	135	32.9
MS-2	119	32.2
VS-2	319	55.3
CS-2	74	26.6
WS-2	42	21.7
WC-2	56	22.4
MH-2	51	22.4

Table 13 Thickness to be implemented for each type of aggregate to obtain a thermal resistance of 7 m².K/W according to modelling results.

These values are consistent with a lost attic space implementation. Only the relatively dense vine shoot seems unsuitable for this type of insulation, given the thickness (and therefore the corresponding load) required to obtain good insulating capacity.

It should be recalled that these values are derived exclusively from the following input data: aggregate particle porosity and particle density. For simplification, the bulk material has been considered unpacked (bulk density), but the model also allows particle compaction to be considered. Once the basic characterization has been carried out, several thermally equivalent solutions can be supplied using different aggregates depending on their availability.

Finally, to take the discrepancy highlighted between the experimental and modelled values for model R (used for sunflower pith) and model B (used for the other aggregates) into account, increasing the thicknesses in Table 13 by 10 % may be recommended.

For clarification and to summarize the procedure that led to the proposal of equivalent constructive solutions from different plant aggregates, a diagram is provided in Figure 9.

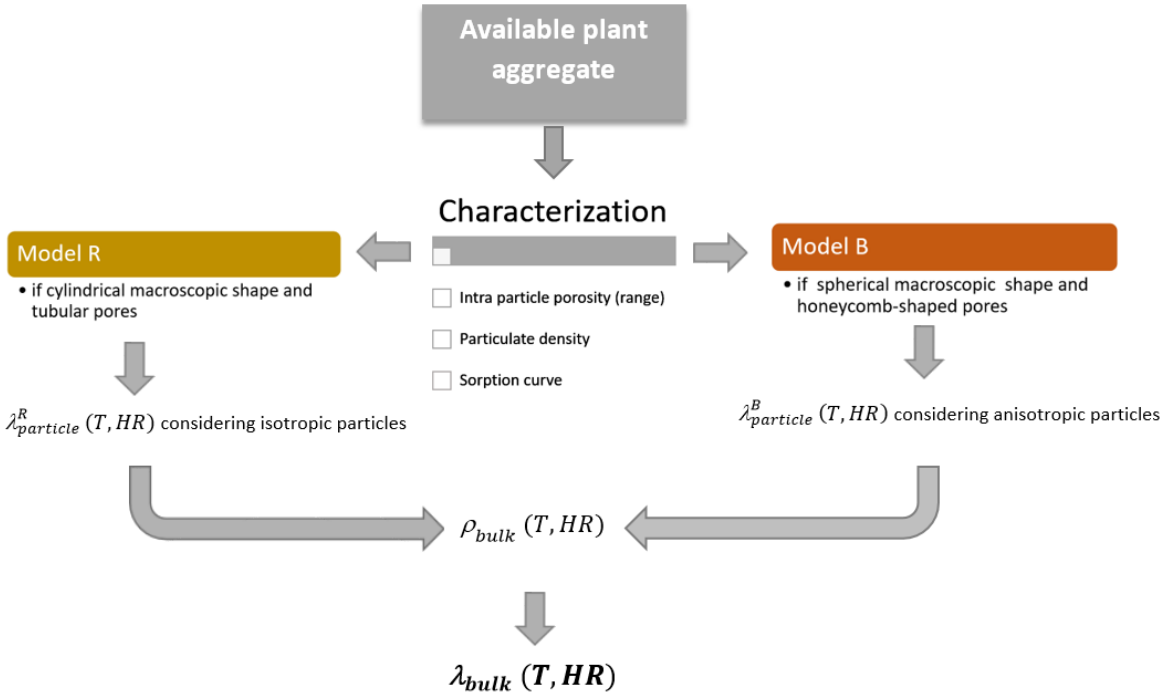

Figure 9. Summary diagram of the proposed approach for predicting the thermal conductivity of bulk aggregates based on a basic characterization of the aggregate under consideration.

5. Conclusion

In this work, a multiscale study has been developed that enables issues from the pore scale to the bulk material scale to be addressed for plant aggregates. Considering the original scale of a single particle of plant aggregate extends the scope of modelling of the insulating capacity of bio-based building materials. A wide range of plant granules has been considered (hemp shiv, flax shiv, sunflower pith and bark, miscanthus stem, coriander straw, etc.). From the intra particulate porosity, particulate density and sorption curve of one cellulosic aggregate, the thermal particulate conductivities of a single particle have been estimated. Previously, only the value for hemp shiv was available and the ambient conditions were not systematically specified. Given the lack of data available in the literature, this study provides valuable data that can be widely used in other models of thermal conductivity of bio-composites for the entire range of temperatures and relative humidity encountered in use.

Based on particle thermal conductivity and bulk density (loose or compacted), a final homogenization step predicts bulk thermal conductivity. These bulk particles can be used to insulate lost attic spaces or intermediate floors with loose filling. Two models have been developed and discussed to predict the thermal conductivity of loose-fill insulation with lignocellulosic aggregates. They take both the microstructure and macrostructure of plant aggregates into account to best fit the available raw material. Their relevance is clear since the difference between the modelled and experimental values is only 10% in the dry state. Given the lack of available data in the literature, comparison under several relative humidities is quite difficult for the moment. Other experimental work, concerning several aggregates and different relative humidities, may complete this study and support the proposed approach.

Nevertheless, the assumptions and methods used in this study apply to a large range of plant aggregates. The models developed are applicable provided that basic characterizations have been made. It is worth noting that particulate porosity is accessible thanks to the easy-to-implement, inexpensive methods recently developed by Ratsimbazafy [22]. The major interest of our models is to propose an efficient and sufficient multi-scale approach without the need for expensive equipment. Thus, the work aims to encourage the use of locally available plant aggregates since a simple characterization is sufficient to feed the predictive model.

In addition, the modelling results presented led to a new theoretical justification of the well-known linear relation between the thermal conductivity and the density of a material. The role of the binder in bio-based composites was raised and discussed from a new perspective. Lastly, it is suggested that the linear relation is also true from the particle scale. As a result, we can now quantify the impact of changes in the density of the solid particulate skeleton (treatment, ageing, etc.) on the insulating capacity of the plant particle.

This iterative approach provides the opportunity to integrate the effect of variability of the raw material on its insulating capacity. This variability of particulate insulating capacity and of ambient conditions (temperature relative humidity) are both considered at the material scale through the multi-scale modelling approach, and open up new perspectives for the prediction of insulating capacities of materials even though they are made of different aggregates with intrinsic variability due to plant species, geographical location, harvesting period, type of crops, harvesting techniques or production methods. To summarize, this study provides an answer to the problem of taking the variability of the primary resource into account. A simple characterization of the aggregate provides the input data necessary for the successive homogenization proposed here. The analytical relationships make the model easier to apply and should allow wider application. It is now possible to predict the same performance from one site to another even when the locally available raw material is different.

Finally, the particle thermal conductivity data provided in this article could serve as a basis for numerous other works. It is now possible to quantify the impact of a modification of the microstructure (intra-particle porosity) on the insulating capacity of the bio-material. As soon as the thermal conductivity of chemical components other than cellulose is available, it is also possible to estimate how a modification of the particulate solid skeleton (density and/or chemical composition) impacts the thermal properties. Another area of work would be to predict the thermal conductivity at the material scale, such as vegetal concrete or lightened earth by mean-field homogenization. This method has demonstrated its relevance in this study. Moreover, it offers the advantage to be not expensive both in terms of material and calculation time.

This work therefore opens up numerous perspectives concerning modeling thermal behavior of bio-based building materials and makes it possible to consider other aggregates than hemp shiv, which is widely studied but not very available in many territories.

Acknowledgements

The authors want to thank ADEME (Agence française pour le DEveloppement et la Maîtrise de l'Energie, the french Energy Agency) and LOCABATI project for financial support of this study.

References

[1] Z. Duan, “Impact of climate change on the life cycle greenhouse gas emissions of cross-laminated timber and reinforced concrete buildings in China,” *J. Clean. Prod.*, vol. 395, p. 136446, Apr. 2023, doi: 10.1016/j.jclepro.2023.136446.

[2] C. Illankoon and S. C. Vithanage, “Closing the loop in the construction industry: A systematic literature review on the development of circular economy,” *J. Build. Eng.*, vol. 76, p. 107362, Oct. 2023, doi: 10.1016/j.jobe.2023.107362.

[3] M. N. Nwodo and C. J. Anumba, “A review of life cycle assessment of buildings using a systematic approach,” *Build. Environ.*, vol. 162, p. 106290, Sep. 2019, doi: 10.1016/j.buildenv.2019.106290.

[4] J. H. Arehart, J. Hart, F. Pomponi, and B. D’Amico, “Carbon sequestration and storage in the built environment,” *Sustain. Prod. Consum.*, vol. 27, pp. 1047–1063, Jul. 2021, doi: 10.1016/j.spc.2021.02.028.

[5] J. C. Morel, A. Mesbah, M. Oggero, and P. Walker, “Building houses with local materials: means to drastically reduce the environmental impact of construction,” *Build. Environ.*, vol. 36, no. 10, pp. 1119–1126, Dec. 2001, doi: 10.1016/S0360-1323(00)00054-8.

[6] A. Arrigoni, R. Pelosato, P. Melià, G. Ruggieri, S. Sabbadini, and G. Dotelli, “Life cycle assessment of natural building materials: the role of carbonation, mixture components and transport in the environmental impacts of hempcrete blocks,” *J. Clean. Prod.*, vol. 149, Feb. 2017, doi: 10.1016/j.jclepro.2017.02.161.

[7] A. A. Sezer and A. Fredriksson, “Environmental impact of construction transport and the effects of building certification schemes,” *Resour. Conserv. Recycl.*, vol. 172, p. 105688, Sep. 2021, doi: 10.1016/j.resconrec.2021.105688.

[8] S. Arufe, A. Hellouin De Menibus, N. Leblanc, and H. Lenormand, “Effect of retting on hemp shiv physicochemical properties,” *Ind. Crops Prod.*, vol. 171, p. 113911, Nov. 2021, doi: 10.1016/j.indcrop.2021.113911.

[9] E. Antczak, M. Asli, F. Brachelet, F. Brue, and D. Defer, “Etude du comportement hygrothermique d’anas de lin utilisés comme isolant en vrac de combles perdus,” 2018.

[10] A. Laborel-Préneron, C. Magniont, and J.-E. Aubert, “Characterization of Barley Straw, Hemp Shiv and Corn Cob as Resources for Bioaggregate Based Building Materials,” *Waste Biomass Valorization*, vol. 9, no. 7, pp. 1095–1112, Jul. 2018, doi: 10.1007/s12649-017-9895-z.

[11] M. Lagouin, “Caractérisation et optimisation multiphysiques d’une paroi bicouche bio et géosourcée,” These de doctorat, Toulouse 3, 2020. Accessed: Oct. 01, 2022. [Online]. Available: https://www.theses.fr/2020TOU30258

[12] “FAO Cereal Supply and Demand Brief | World Food Situation | Food and Agriculture Organization of the United Nations.” Accessed: May 30, 2023. [Online]. Available: https://www.fao.org/worldfoodsituation/csdb/en/

[13] J.-M. Faurès, J. Hoogeveen, and J. Bruinsma, “THE FAO IRRIGATED AREA FORECAST FOR 2030”.

[14] M. Donner, A. Verniquet, J. Broeze, K. Kayser, and H. De Vries, “Critical success and risk factors for circular business models valorising agricultural waste and by-products,” *Resour. Conserv. Recycl.*, vol. 165, p. 105236, Feb. 2021, doi: 10.1016/j.resconrec.2020.105236.

[15] E. Loizou, C. Karelakis, K. Galanopoulos, and K. Mattas, “The role of agriculture as a development tool for a regional economy,” *Agric. Syst.*, vol. 173, pp. 482–490, Jul. 2019, doi: 10.1016/j.agsy.2019.04.002.

[16] T. A. Toop, S. Ward, T. Oldfield, M. Hull, M. E. Kirby, and M. K. Theodorou, “AgroCycle – developing a circular economy in agriculture,” *Energy Procedia*, vol. 123, pp. 76–80, Sep. 2017, doi: 10.1016/j.egypro.2017.07.269.

[17] Université de Toulouse, INSA, UPS, LMDC (Laboratoire Matériaux et Durabilité des Constructions), 135 avenue de Rangueil, 31 077 Toulouse Cedex 04, France *et al.*, “A Review of the Multi-Physical Characteristics of Plant Aggregates and Their Effects on the Properties of

Plant-Based Concrete," *Recent Prog. Mater.*, vol. 03, no. 02, pp. 1–1, Mar. 2021, doi: 10.21926/rpm.2102026.
[18] L. Wang, H. Lenormand, H. Zmamou, and N. Leblanc, "Effect of variability of hemp shiv on the setting of lime hemp concrete," *Ind. Crops Prod.*, vol. 171, p. 113915, Nov. 2021, doi: 10.1016/j.indcrop.2021.113915.
[19] T. Vinceslas, T. Colinart, E. Hamard, A. H. de Ménibus, T. Lecompte, and H. Lenormand, "Light earth performances for thermal insulation: application to earth-hemp," *Acad. J. Civ. Eng.*, vol. 35, no. 2, Art. no. 2, Jun. 2017, doi: 10.26168/icbbm2017.26.
[20] S. Amziane, F. Collet, M. Lawrence, C. Magniont, V. Picandet, and M. Sonebi, "Recommendation of the RILEM TC 236-BBM: characterisation testing of hemp shiv to determine the initial water content, water absorption, dry density, particle size distribution and thermal conductivity," *Mater. Struct.*, vol. 50, no. 3, p. 167, Apr. 2017, doi: 10.1617/s11527-017-1029-3.
[21] H. H. Ratsimbazafy, A. Laborel-Preneron, C. Magniont, and P. Evon, "Comprehensive Characterization of Agricultural By-Products for Bio-Aggregate Based Concrete," *Constr. Technol. Archit.*, vol. 1, pp. 77–84, Jan. 2022, Accessed: Apr. 12, 2023. [Online]. Available: https://doi.org/10.4028/www.scientific.net/CTA.1.77
[22] H. H. Ratsimbazafy, "Évaluation du potentiel de co-produits agricoles locaux valorisables dans le domaine des matériaux de construction (PALOMAC)," These de doctorat, Toulouse 3, 2022. Accessed: Oct. 01, 2022. [Online]. Available: https://www.theses.fr/2022TOU30005
[23] M. Lagouin *et al.*, "Structuration d'une filière de valorisation transfrontalière des tiges de maïs et de tournesol pour la construction," *Acad. J. Civ. Eng.*, vol. 40, no. 1, Art. no. 1, Jun. 2022, doi: 10.26168/ajce.40.1.66.
[24] V. Cérézo, "Propriétés mécaniques, thermiques et acoustiques d'un matériau à base de particules végétales : approche expérimentale et modélisation théorique," These de doctorat, Lyon, INSA, 2005. Accessed: Oct. 03, 2022. [Online]. Available: https://www.theses.fr/2005ISAL0037
[25] R. Walker and S. Pavía, "Moisture transfer and thermal properties of hemp–lime concretes," *Constr. Build. Mater.*, vol. 64, pp. 270–276, Aug. 2014, doi: 10.1016/j.conbuildmat.2014.04.081.
[26] A. Hussain, J. Calabria-Holley, M. Lawrence, and Y. Jiang, "Hygrothermal and mechanical characterisation of novel hemp shiv based thermal insulation composites," *Constr. Build. Mater.*, vol. 212, pp. 561–568, Jul. 2019, doi: 10.1016/j.conbuildmat.2019.04.029.
[27] T. Pierre, M. Carin, M. Courtois, and P. Carré, "Transient infrared thermography to characterise thermal properties of millimetre-sized hemp shiv," *Quant. InfraRed Thermogr. J.*, vol. 17, pp. 1–15, Jun. 2019, doi: 10.1080/17686733.2019.1609274.
[28] S. Dartois, S. Mom, H. Dumontet, and A. B. Hamida, "An iterative micromechanical modeling to estimate the thermal and mechanical properties of polydisperse composites with platy particles: Application to anisotropic hemp and lime concretes," *Constr. Build. Mater.*, vol. 152, p. 661, 2017, doi: 10.1016/j.conbuildmat.2017.06.181.
[29] A. D. Tran-Le, S.-T. Nguyen, and T. Langlet, "A novel anisotropic analytical model for effective thermal conductivity tensor of dry lime-hemp concrete with preferred spatial distributions," *Energy Build.*, vol. 182, pp. 75–87, Jan. 2019, doi: 10.1016/j.enbuild.2018.09.043.
[30] P. A. Chabriac, E. Gourdon, P. Gle, A. Fabbri, and H. Lenormand, "Agricultural by-products for building insulation: Acoustical characterization and modeling to predict micro-structural parameters," *Constr. Build. Mater.*, vol. 112, pp. 158–167, Jun. 2016, doi: 10.1016/j.conbuildmat.2016.02.162.
[31] A. M. Almusawi, "Mise en œuvre et optimisation des propriétés d'une structure sandwich en matériaux biosourcés (fibres et bois de chanvre) avec une matrice en polystyrène expansé pour le bâtiment," phdthesis, Université Bourgogne Franche-Comté, 2017. Accessed: Nov. 14, 2022. [Online]. Available: https://tel.archives-ouvertes.fr/tel-01870446
[32] W. Stelte, C. Clemons, J. K. Holm, J. Ahrenfeldt, U. B. Henriksen, and A. R. Sanadi, "Thermal transitions of the amorphous polymers in wheat straw," *Ind. Crops Prod.*, vol. 34, no. 1, pp. 1053–1056, Jul. 2011, doi: 10.1016/j.indcrop.2011.03.014.

[33] G. Huang, A. Abou-Chakra, J. Absi, and S. Geoffroy, “Optimization of mechanical properties in anisotropic bio-based building materials by a multiscale homogenization model,” *J. Build. Eng.*, vol. 57, p. 104890, Oct. 2022, doi: 10.1016/j.jobe.2022.104890.
[34] S. Amziane, F. Collet, M. Lawrence, C. Magniont, V. Picandet, and M. Sonebi, “Recommendation of the RILEM TC 236-BBM: characterisation testing of hemp shiv to determine the initial water content, water absorption, dry density, particle size distribution and thermal conductivity,” *Mater. Struct.*, vol. 50, no. 3, p. 167, Jun. 2017, doi: 10.1617/s11527-017-1029-3.
[35] M. Lagouin, P. Sénéchal, P. Moonen, C. Magniont, J.-E. E. Aubert, and A. Laborel-Préneron, “Potential of X-ray tomography for the exploration of vegetal concretes’ porous structure,” presented at the 3rd International Conference on Bio-Based Building Materials (ICBBM), Jun. 2019. Accessed: Apr. 03, 2023. [Online]. Available: https://hal.science/hal-02175817
[36] M. Viel, F. Collet, and C. Lanos, “Chemical and multi-physical characterization of agro-resources’ by-product as a possible raw building material,” *Ind. Crops Prod.*, vol. 120, pp. 214–237, Sep. 2018, doi: 10.1016/j.indcrop.2018.04.025.
[37] F. Bennai, “Étude des mécanismes de transferts couplés de chaleur et d’humidité dans les matériaux poreux de construction en régime insaturé,” These de doctorat, La Rochelle, 2017. Accessed: Oct. 01, 2022. [Online]. Available: https://www.theses.fr/2017LAROS013
[38] C. Magniont, G. Escadeillas, M. Coutand, and C. Oms, “Use of plant aggregates in building ecomaterials,” *Eur. J. Environ. Civ. Eng.*, vol. 16, pp. s17–s33, Jun. 2012, doi: 10.1080/19648189.2012.682452.
[39] Y. Jiang, M. Lawrence, M. P. Ansell, and A. Hussain, “Cell wall microstructure, pore size distribution and absolute density of hemp shiv,” *R. Soc. Open Sci.*, vol. 5, no. 4, p. 171945, Apr. 2018, doi: 10.1098/rsos.171945.
[40] N. Mati-Baouche, “Conception d’isolants thermiques à base de broyats de tiges de tournesol et de liants polysaccharidiques”.
[41] M. S. Abbas, “Caractérisations multi-physiques des mortiers bio-sourcés isolants et modélisation de leurs impacts sur les transferts hygrothermiques à l’échelle des parois : application aux bétons de moelles végétales,” These de doctorat, Lyon, 2021. Accessed: Oct. 01, 2022. [Online]. Available: https://www.theses.fr/2021LYSET003
[42] “Acoustic performance and microstructural analysis of bio-based lightweight concrete containing miscanthus | Elsevier Enhanced Reader.” Accessed: Feb. 20, 2023. [Online]. Available: https://reader.elsevier.com/reader/sd/pii/S0950061817319840?token=B63F2F72E73642D8D46F73FEAEFF2138A2B7186819D7D4A83EB77695D2080B291C8A746FDB47A23C21A647CC13F804DB&originRegion=eu-west-1&originCreation=20230220121317
[43] T. Colinart, T. Vinceslas, H. Lenormand, A. H. D. Menibus, E. Hamard, and T. Lecompte, “Hygrothermal properties of light-earth building materials,” *J. Build. Eng.*, vol. 29, p. 101134, May 2020, doi: 10.1016/j.jobe.2019.101134.
[44] A. Bourdot *et al.*, “Characterization of a hemp-based agro-material: Influence of starch ratio and hemp shive size on physical, mechanical, and hygrothermal properties,” *Energy Build.*, vol. 153, pp. 501–512, Oct. 2017, doi: 10.1016/j.enbuild.2017.08.022.
[45] T. Nguyen, V. Picandet, T. Lecompte, P. Carre, S. Amziane, and C. Baley, *Etude de la compacité du béton de chanvre sur leurs caractéristiques mécaniques et thermiques*. 2009.
[46] “Characterization of flax lime and hemp lime concretes: Hygric properties and moisture buffer capacity | Elsevier Enhanced Reader.” Accessed: Feb. 20, 2023. [Online]. Available: https://reader.elsevier.com/reader/sd/pii/S037877881400974 8?token=3173A398ADC706AF6AB13C2A9CB7366E2964E8DD2A0C102BD9F24585EA3239FFA2252A28A12D12DAA50BC8559C798EF6&originRegion=eu-west-1&originCreation=20230220152914
[47] S. Rosa Latapie, A. Abou-Chakra, and V. Sabathier, “Microstructure of Bio-Based Building Materials: New Insights into the Hysteresis Phenomenon and Its Consequences,” *Buildings*, vol. 13, no. 7, Art. no. 7, Jul. 2023, doi: 10.3390/buildings13071650.

[48] J. D. Eshelby, “The Determination of the Elastic Field of an Ellipsoidal Inclusion, and Related Problems,” *Proc. R. Soc. Lond. Ser. A*, vol. 241, pp. 376–396, Aug. 1957, doi: 10.1098/rspa.1957.0133.
[49] T. Mori and K. Tanaka, “Average stress in matrix and average elastic energy of materials with misfitting inclusions,” *Acta Metall.*, vol. 21, no. 5, pp. 571–574, May 1973, doi: 10.1016/0001-6160(73)90064-3.
[50] S. Mom, S. Dartois, A. B. Hamida, H. Dumontet, and H. Boussa, “Modélisation multi-échelles du comportement thermique du béton de chanvre, influence de la morphologie sur le comportement effectif,” *Matér. Tech.*, vol. 99, no. 6, Art. no. 6, 2011, doi: 10.1051/mattech/2011116.
[51] T. Pierre, T. Colinart, and P. Glouannec, “Measurement of Thermal Properties of Biosourced Building Materials,” *Int. J. Thermophys.*, vol. 35, no. 9, pp. 1832–1852, Oct. 2014, doi: 10.1007/s10765-013-1477-0.
[52] M. Antlauf, N. Boulanger, L. Berglund, K. Oksman, and O. Andersson, “Thermal Conductivity of Cellulose Fibers in Different Size Scales and Densities,” *Biomacromolecules*, vol. 22, no. 9, pp. 3800–3809, Sep. 2021, doi: 10.1021/acs.biomac.1c00643.
[53] S. Rosa Latapie, M. Lagouin, V. Sabathier, and A. Abou-Chakra, “From aggregate to particleboard: A new multi-scale model approach to thermal conductivity in bio-based materials,” *J. Build. Eng.*, vol. 78, p. 107664, Nov. 2023, doi: 10.1016/j.jobe.2023.107664.
[54] S. T. Nguyen, A. D. Tran-Le, M. N. Vu, Q. D. To, O. Douzane, and T. Langlet, “Modeling thermal conductivity of hemp insulation material: A multi-scale homogenization approach,” *Build. Environ.*, vol. 107, pp. 127–134, Oct. 2016, doi: 10.1016/j.buildenv.2016.07.026.
[55] P. T. Tsilingiris, “Thermophysical and transport properties of humid air at temperature range between 0 and 100°C,” *Energy Convers. Manag.*, vol. 49, pp. 1098–1110, May 2008, doi: 10.1016/j.enconman.2007.09.015.
[56] J. P. Laurent and C. Guerre-Chaley, “Influence de la teneur en eau et de la température sur la conductivité thermique du béton cellulaire autoclavé,” *Mater. Struct.*, vol. 28, no. 8, pp. 464–472, Oct. 1995, doi: 10.1007/BF02473166.
[57] T. Pham, J. Férec, V. Picandet, P. Tronet, J. Costa, and P. Pilvin, *Etude expérimentale et numérique de la conductivité thermique d’un composite chaux–chanvre*. 2012.
[58] M. S. Abbas, F. McGregor, A. Fabbri, and M. Y. Ferroukhi, “The use of pith in the formulation of lightweight bio-based composites: Impact on mechanical and hygrothermal properties,” *Constr. Build. Mater.*, vol. 259, p. 120573, Oct. 2020, doi: 10.1016/j.conbuildmat.2020.120573.
[59] T. Behzad and M. Sain, “Measurement and prediction of thermal conductivity for hemp fiber reinforced composites,” *Polym. Eng. Sci.*, vol. 47, no. 7, pp. 977–983, 2007, doi: 10.1002/pen.20632.
[60] G. Huang, A. Abou-Chakra, S. Geoffroy, and J. Absi, “A multiscale homogenization model on thermal conductivity of bio-based building composite considering anisotropy, imperfect interface and moisture,” *Constr. Build. Mater.*, vol. 377, p. 131156, May 2023, doi: 10.1016/j.conbuildmat.2023.131156.
[61] C. Piegay, “Approche conjointe acoustique et thermique pour l’optimisation des laines végétales du bâtiment,” 2019.
[62] M. Chabannes, V. Nozahic, and S. Amziane, “Design and multi-physical properties of a new insulating concrete using sunflower stem aggregates and eco-friendly binders,” *Mater. Struct.*, vol. 48, no. 6, pp. 1815–1829, Jun. 2015, doi: 10.1617/s11527-014-0276-9.
[63] V. Nozahic, “Vers une nouvelle démarche de conception des bétons de végétaux lignocellulosiques basée sur la compréhension et l’amélioration de l’interface liant / végétal: application à des granulats de chenevotte et de tige de tournesol associés à un liant ponce / chaux”.
[64] C. Magniont, “Contribution à la formulation et à la caractérisation d’un écomatériau de construction à base d’agroressources,” These de doctorat, Toulouse 3, 2010. Accessed: Oct. 04, 2022. [Online]. Available: https://www.theses.fr/2010TOU30101

[65] Y. Brouard, N. Belayachi, D. Hoxha, N. Ranganathan, and S. Méo, “Mechanical and hygrothermal behavior of clay – Sunflower (Helianthus annuus) and rape straw (Brassica napus) plaster bio-composites for building insulation,” *Constr. Build. Mater.*, vol. 161, pp. 196–207, Feb. 2018, doi: 10.1016/j.conbuildmat.2017.11.140.
[66] F. Collet and S. Prétot, “THERMAL CONDUCTIVITY OF HEMP CONCRETES: VARIATION WITH FORMULATION, DENSITY AND WATER CONTENT,” *Constr. Build. Mater.*, vol. 65, pp. 612–619, 2014, doi: 10.1016/j.conbuildmat.2014.05.039.
[67] J. Page, M. Sonebi, and S. Amziane, “Design and multi-physical properties of a new hybrid hemp-flax composite material,” *Constr. Build. Mater.*, vol. 139, pp. 502–512, May 2017, doi: 10.1016/j.conbuildmat.2016.12.037.
[68] P. Glé *et al.*, “Densities of hemp shiv for building: From multiscale characterisation to application,” *Ind. Crops Prod.*, vol. 164, p. 113390, Jun. 2021, doi: 10.1016/j.indcrop.2021.113390.
[69] D. Kumar, M. Alam, P. X. W. Zou, J. G. Sanjayan, and R. A. Memon, “Comparative analysis of building insulation material properties and performance,” *Renew. Sustain. Energy Rev.*, vol. 131, p. 110038, Oct. 2020, doi: 10.1016/j.rser.2020.110038.
[70] C. Rabbat, S. Awad, A. Villot, D. Rollet, and Y. Andrès, “Sustainability of biomass-based insulation materials in buildings: Current status in France, end-of-life projections and energy recovery potentials,” *Renew. Sustain. Energy Rev.*, vol. 156, p. 111962, Mar. 2022, doi: 10.1016/j.rser.2021.111962.